

DETECTING AND APPROXIMATING REDUNDANT COMPUTATIONAL BLOCKS IN NEURAL NETWORKS

Anonymous authors

Paper under double-blind review

ABSTRACT

Deep neural networks often learn similar internal representations, both across different models and within their own layers. While inter-network similarities have enabled techniques such as model stitching and merging, intra-network similarities present new opportunities for designing more efficient architectures. In this paper, we investigate the emergence of these internal similarities across different layers in diverse neural architectures, showing that similarity patterns emerge independently of the dataset used. We introduce a simple metric, Block Redundancy, to detect redundant blocks, providing a foundation for future architectural optimization methods. Building on this, we propose Redundant Blocks Approximation (RBA), a general framework that identifies and approximates one or more redundant computational blocks using simpler transformations. We show that the transformation \mathcal{T} between two representations can be efficiently computed in closed-form, and it is enough to replace the redundant blocks from the network. RBA reduces model parameters and time complexity while maintaining good performance. We validate our method on classification tasks in the vision domain, using a variety of pretrained foundational models and datasets.

1 INTRODUCTION

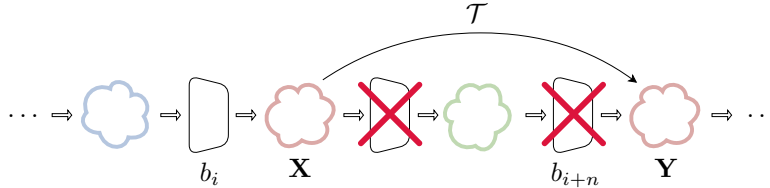


Figure 1: **Framework Description.** Given two latent spaces \mathbf{X} and \mathbf{Y} representing respectively the output of blocks b_i and b_{i+n} for a subset of n data points from the training set, we approximate a transformation matrix \mathcal{T} such that: $\mathbf{Y} \approx \mathbf{Y}' = \mathcal{T}(\mathbf{X})$ to recover a representation $\mathbf{Y}' \approx \mathbf{Y}$.

As Neural Networks (NNs) grow in size and complexity, their demand for computational resources has become a significant bottleneck. Despite the impressive performance of large models, they often come with substantial trade-offs, such as slower inference times and increased memory and power consumption. This has led to a growing interest in methods that can reduce model complexity without sacrificing performance. However, most approaches to mitigating these challenges either require additional training or complex fine-tuning, or they result in a non-trivial loss in performance. However, recent research showed that there exists internal representation similarities within and between NNs. Thus, many layers or components within these networks may perform similar functions or yield highly correlated outputs, suggesting the potential for simplifying these networks. Understanding and leveraging these internal similarities can open up new opportunities for reducing model size, enhancing inference speed, and improving computational efficiency.

In this paper, we address two key research questions: (i) how to identify redundant blocks, and (ii) how to effectively approximate these blocks while preserving the final representations and the network’s overall functionality. To address the first question, we introduce a straightforward metric, the Block Redundancy (BR) score, which helps identifying components that do not contribute significantly to the network’s final representation. By carefully selecting which blocks to approximate, we can ensure

minimal impact on the network’s final output. For the second question, we propose the Redundant Blocks Approximation (RBA), a novel method that leverages internal representation similarities to approximate redundant computational blocks using lightweight transformations, such as linear mappings. Once the blocks that have minimal impact on model functionality are identified, instead of using these redundant blocks in each forward pass (e.g., transformer blocks containing attention and normalization operations), RBA completely replaces them with a simpler transformation. Thanks to this approximation, RBA reduces model parameters and accelerates inference while maintaining the integrity of the final representation produced by the original model.

Our main contributions are as follows:

- We provide a comprehensive analysis of internal representation similarities across various pretrained foundation models, revealing consistent patterns between blocks within each architecture, independent of the dataset (Figures 2 and 7 to 8).
- We show that a simple metric such as the MSE is enough for assessing the redundancy of individual blocks within a NN (Figure 3).
- We introduce RBA, a general framework for identifying and approximating redundant computational blocks in NNs using simpler transformations (e.g., linear), reducing model parameters and complexity with minimal to no impact on the produced representations (Figure 1).
- We validate our method on vision-based classification tasks using diverse pretrained models and datasets, demonstrating its applicability and effectiveness across different architectures and datasets (Tables 1, 6 and 7).

2 RELATED WORK

Measuring Similarities. A range of metrics have been introduced to assess the similarity between latent spaces generated by different NNs Klabunde et al. (2023); Ballester et al. (2023). One established approach is Canonical Correlation Analysis (CCA) (Hotelling, 1992), known for its invariance to linear transformations. Variants of CCA, such Singular Value Decomposition (SVD) and Singular Value CCA (SVCCA) (Raghu et al., 2017), aim to enhance robustness, while techniques like Projection Weighted CCA (PWCCA) (Morcos et al., 2018) mitigate sensitivity to small perturbations. Another widely used metric, Centered Kernel Alignment (CKA) (Kornblith et al., 2019), captures the similarity between latent spaces while ignoring orthogonal transformations. However, recent work (Davari et al., 2022) highlights that this metric can be sensitive to shifts in the latent space. Additionally, Barannikov et al. (2021) proposes a method to compare two data representations by measuring the multi-scale topological dissimilarity, while Fumero et al. (2024) leverages the principles of spectral geometry to model and analyze the relationships between distinct latent spaces.

Leveraging Similarities. Analyzing the similarities between internal representations, both within and across NNs, has received significant attention in recent research. Valeriani et al. (2024) examines the intrinsic dimensions and neighbor compositions of representations in various transformer models. Similarly, Kvinge et al. (2022) explores how models process different variations of data points across layers, while Nguyen et al. (2020) investigates how changes in network depth and width impact hidden representations, revealing characteristic block structures. Finally, Crisostomi et al. (2023) investigates under what assumptions two latent spaces be merged into one. All these insights have been applied across various contexts. Moschella et al. (2023) constructs a unified space shared by different NNs, enabling zero-shot stitching of independently trained models across different modalities Norelli et al. (2023), even without explicit assumptions on the transformation class that connects the latent manifold embeddings Cannistraci et al. (2024) or with partial correspondence within the latent spaces Cannistraci et al. (2023). While Ricciardi et al. (2023) proves the feasibility of zero-shot stitching between encoders and policies trained on different environmental variations. Other works Lähner & Moeller (2024); Maiorca et al. (2024) demonstrate that representations learned by distinct NNs can be aligned using simple transformations. Finally, Tang et al. (2023) leverages similarities in unified visual-language models to dynamically skip layers in both encoders and decoders.

Architectural Efficiency. While large-scale models with billions or even trillions of parameters continue to achieve state-of-the-art performance, their growth comes with trade-offs, including slower inference times and significantly higher computational costs. To address these issues, various

techniques have been developed, such as early exiting and model pruning. Early exit strategies, which introduce intermediate output layers at different stages of the network, have been shown to improve efficiency and reduce inference time (Xin et al., 2020; Zhou et al., 2020; Yu et al., 2022). However, this approach requires the additional training of intermediate classifiers to enable exits at predefined layers. On the other hand, model pruning reduces the computational load of Deep Neural Network (DNN) by either removing individual weights based on certain criteria (Ma et al., 2023; Liao et al., 2023) or eliminating or compressing larger structural components such as channels or attention heads (Zhang & He, 2020; Sajjad et al., 2023; Venkataramanan et al., 2024; Zhang et al., 2024; Bai et al., 2023). Although effective, this approach usually requires first training the full model in its dense form, followed by multiple iterations of pruning and retraining or training the pruned model from scratch.

Instead of removing layers or components, we focus on identifying redundant computational blocks within the network and replacing them with lightweight transformations. Unlike other approaches, RBA is an *architecture-agnostic* method to reduce model complexity and computational overhead *without the need for additional training or fine-tuning* while still maintaining competitive performance.

3 REDUNDANT BLOCKS APPROXIMATION

The core principle of our approach, RBA, is to detect similar representations within NNs, identifying redundant blocks, and approximate them with simpler transformations instead of executing the entire DNN. A visual overview is provided in Figure 1.

In this section, we first show how to identify redundant blocks, and how to effectively approximate their representations while preserving the network’s overall functionality.

Identifying Redundant Representations. We hypothesize that certain foundation model architectures, such as Vision Transformers (ViTs), may contain redundant blocks that produce similar representations. This redundancy may stem from overparameterization or task-specific characteristics. In this context, a “block” refers to a self-contained unit in the model that typically contains several layers, such as self-attention, normalization, or feed-forward layers, but functions as a cohesive unit.

To quantify redundancy, we introduce a simple metric called Block Redundancy (BR), which measures the degree of change in internal representations between blocks. This helps to identify essential blocks versus those that contribute minimally to the overall model.

Let B represent the total number of blocks in the model, and let $\mathbf{h}^{(b)}$ denote the internal representation (i.e., the output) of block b , where $b \in 1, 2, \dots, B$. For a given subset of the training data \mathcal{D}_{sub} , we compute the representations $\mathbf{h}^{(b)}(x)$ for each input $x \in \mathcal{D}_{\text{sub}}$. The BR for block b is defined as the negative Mean Squared Error (MSE) between the output representations of blocks b and $b - 1$:

$$\text{BR}(b) = -\frac{1}{|\mathcal{D}_{\text{sub}}|} \sum_{x \in \mathcal{D}_{\text{sub}}} \left\| \mathbf{h}^{(b)}(x) - \mathbf{h}^{(b-1)}(x) \right\|_2^2 \quad (1)$$

A higher $\text{BR}(b)$ indicates a minimal change between the outputs of block b and the preceding block $b - 1$, suggesting a potential redundancy in block b . Conversely, a lower $\text{BR}(b)$ implies that block b plays a significant role in transforming the internal representations.

By systematically evaluating the BR for each block, we can identify redundant components that can be simplified, enabling a reduction in the NN’s complexity without compromising the original final representation or its performance.

Approximating Redundant Blocks. After identifying redundant representations using BR, the next step is to approximate their outputs through more computationally efficient transformations, rather than directly removing the blocks. While this approach applies to consecutive blocks such as b_i and b_{i+1} , it generalizes naturally to non-consecutive blocks as well. Specifically, for any block b_i and block b_{i+n} (where $n \geq 1$), our method enables the approximation of the output of block b_{i+n} from the output of block b_i , provided they exhibit low BR scores. This allows us to skip the computation of blocks $b_{i+1}, b_{i+2}, \dots, b_{i+n}$, effectively reducing the overall computation.

Let $\mathbf{X} \in \mathbb{R}^{n \times d_1}$ represent the output of block b_i for a subset of n data points from the training set, where d_1 is the dimensionality of the latent space. Similarly, let $\mathbf{Y} \in \mathbb{R}^{n \times d_2}$ represent the output of

block b_{i+n} for the same subset of data points, with d_2 being the dimensionality of the latent space at block b_{i+n} . Our objective is to find a function $\mathcal{T} : \mathbb{R}^{d_1} \rightarrow \mathbb{R}^{d_2}$ such that:

$$\mathbf{Y} \approx \mathcal{T}(\mathbf{X})$$

In this work, we consider \mathcal{T} to be a linear transformation (\mathbf{T}) that can be estimated by minimizing the squared error between the transformed output of block b_i and the actual output of block b_{i+n} , which can be solved using least squares:

$$\mathbf{T} = \arg \min_{\mathcal{T}} \|\mathbf{Y} - \mathcal{T}(\mathbf{X})\|_2^2$$

This optimization problem allows for a closed-form solution that efficiently computes the optimal transformation \mathbf{T} . The solution bypasses the computation of any redundant blocks between b_i and b_{i+n} , replacing them with \mathbf{T} . This approximation results in a significant reduction in computational complexity, as one or more full transformer block consisting of multi-head self-attention and feed-forward layers can be replaced by a low-cost linear transformation.

To sum up, the overall pipeline of our approach comprises two main stages:

1. **Redundancy Identification:** We apply the BR metric to identify redundant blocks across the model based on their contribution to the transformation of internal representations.
2. **Block Approximation:** For blocks deemed redundant, we compute an efficient linear approximation, using the transformation matrix \mathbf{T} to bypass these blocks.

This process reduces model parameters and computational complexity with minimal impact on the resulting representations, as shown in Figures 3, 4 and 9 to 12. Additionally, it is possible to train any downstream linear classifier on top of the simplified model for the desired task, retaining the original architecture’s overall structure while significantly decreasing the number of parameters and computation costs, as shown in Tables 1, 2 and 6 to 8.

4 EXPERIMENTS

In this section, we analyze the representation of foundation pre-trained models and we show quantitative experiments to evaluate the effectiveness of our proposed framework. We begin by empirically motivating our study in Section 4.1, where we analyze the similarity between different blocks of pretrained foundation models for image classification. Then in Section 4.2, we assess the impact of approximating blocks on latent representations and explore the correlation between layer approximations and high BR. Finally in Section 4.3, we conduct quantitative experiments on the image classification task to further evaluate the performance of our framework across various models and datasets, demonstrating its general applicability and effectiveness.

4.1 BLOCK SIMILARITIES

Experimental Setting. In this section, we analyze the latent spaces generated by pretrained foundational models in the vision domain. Our analysis focuses on five distinct transformer-based models: ViT-S, ViT-B, DiNO-S, DiNO-B, and DeiT-S. We evaluate their similarities using four well-known datasets: CIFAR-10, CIFAR-100 (Krizhevsky et al., 2009), MNIST (Deng, 2012), and F-MNIST (Xiao et al., 2017). Since these models classify input based on the representation of the [CLS] token, the analysis is conducted using the [CLS] token from each block, rather than the full representation. This ensures that the analysis remains aligned with the key components of the model’s final predictions. This flexibility enables the method to adapt to different model architectures and tasks, where tokens other than the [CLS] may hold more relevant information. Model and dataset details can be found in Table 4 and Table 5, respectively.

Results and Analysis. Figure 2 presents the cosine similarity matrices between blocks of the ViT-B and DiNO-S models on MNIST and CIFAR-100. These matrices illustrate the internal block-by-block similarities within each architecture. Our results reveal that while the patterns of similarity vary across architectures, they remain consistent across different datasets. This suggests that the similarity structure between computational blocks is predominantly influenced by the model architecture itself, rather than the specific dataset used. This finding aligns with observations from Nguyen et al. (2020),

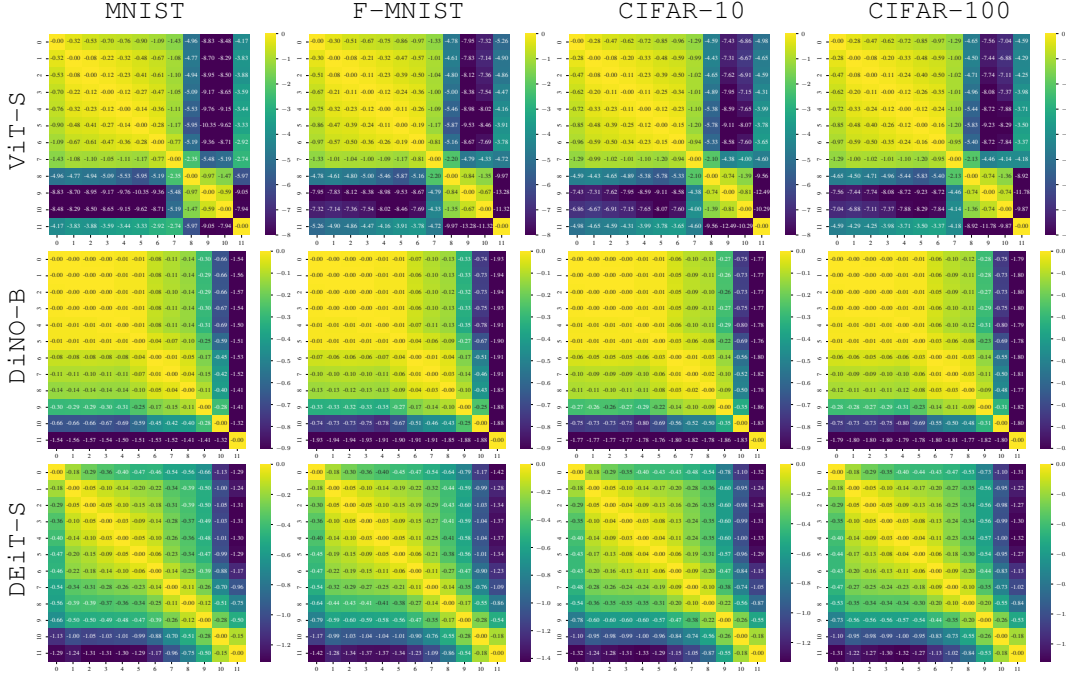


Figure 2: **Representation Redundancies.** BR matrices illustrating the internal block-by-block redundancies in ViT-S, DiNO-B, and DEiT-S models across four datasets: MNIST, F-MNIST, CIFAR-10, and CIFAR-100. Each heatmap quantifies the BR metric between internal representations of different blocks using the Classify token (ICLS) token, providing insights into redundancy in foundation pretrained models. The matrices reveal that the similarity structure between computational blocks is predominantly influenced by the model architecture itself, rather than the specific dataset. Please refer to Figures 7 and 8 for additional results using other metrics and models.

where wide and deep trained from scratch models tend to exhibit a distinctive “block structure” in their representations, linked to model overparameterization. Our results extend this observation by showing that block structures also emerge in pretrained foundation models, with their presence primarily dependent on the architecture. Please refer to Figures 7 and 8 for additional results.

Takeaway. The representation patterns generated by pretrained models are primarily determined by the architecture, and remain consistent across different datasets.

4.2 REDUNDANT BLOCK APPROXIMATION

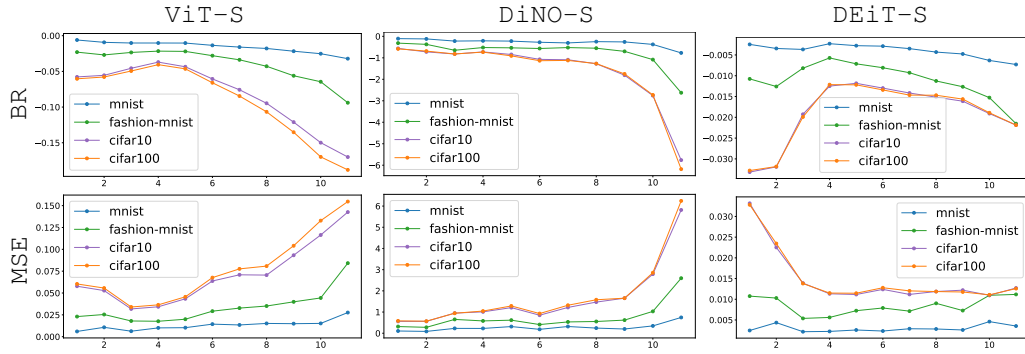


Figure 3: **Block Redundancy vs. Representation Similarity.** This figure illustrates the correlation between the BR metric when approximating the i^{th} block and the MSE between the last layer representations of the original encoder and the approximated encoder. Each column corresponds to a different model (ViT-S, DiNO-S, DEiT-S), while the various curves represent different datasets.

Experimental Setting. In Section 4.1, we empirically demonstrate that different blocks in pretrained models exhibit similarities. To further investigate this, introduce the Block Redundancy metric. As illustrated in Equation (1), this metric measures the level of redundancy of a block: a high score indicates minimal change between two blocks output, suggesting that the second block may be redundant. Conversely, a low score implies that the second block contributes significantly to the final prediction. After identifying redundant blocks, we restructure the models accordingly to reduce their complexity and parameter count. These redundant blocks are approximated using a shared linear transformation applied across all tokens, based on a subset of 3,000 training samples. We compute BR scores for each block across different datasets and pretrained encoders: ViT-S, DiNO-S, DEiT-S, utilizing MNIST, F-MNIST, CIFAR-10, and CIFAR-100. Additionally, we compute the MSE between the representations of the last layer in the original model and the RBA model when skipping the i^{th} block. We also visualize the Principal Component Analysis (PCA) projections of these representations when specific blocks are approximated to assess the impact on representation fidelity.

Quantitative Analysis. As illustrated in Figure 3, in most cases, the BR decreases as the block depth increases. This suggests that approximating the final blocks would lead to significant changes in the final representations, indicating their critical role in maintaining similar final representations. However, in the case of DEiT-S, the trend is reversed. Here, the BR is higher in the central blocks and lower in the initial ones. This is confirmed by the dissimilarity (MSE) between the last-layer representations, which increases when the earlier blocks are removed in DEiT-S, whereas the opposite is observed in other models. These findings reinforce the intuition behind the BR metric, demonstrating a correlation between BR and the final representation similarity when approximating blocks.

In some instances, such as with the MNIST dataset, the BR scores remain relatively consistent across blocks, indicating that the representations are largely similar one to another. However, for more complex datasets like CIFAR-100, the representations in the final or in the first blocks become increasingly dissimilar, making it advantageous to approximate intermediate blocks. This suggests that the BR metric is influenced not only by the architecture but also by the complexity of the dataset, allowing for targeted approximations that reduce model parameters and complexity without significantly compromising performance.

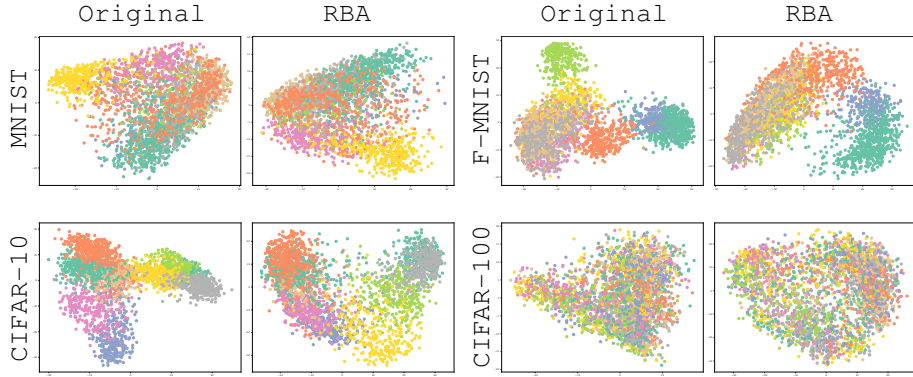


Figure 4: **Last Block Approximation.** PCA visualization of the final layer representations for both the original model and the model with its last block approximated from the preceding one. The representations are generated using the DiNO-S model across four datasets. The plots highlight that in this model, the last layer representations are crucial, making it more effective to approximate earlier blocks instead. Note that for CIFAR-100 (bottom right), only the overall structure of the space can be observed, as the 100 classes make it challenging to distinguish labels based on color. For further results approximating other blocks and using other encoders, refer to Figures 9 to 11.

Qualitative Analysis. To further investigate the relationship between BR and representation (dis)similarity, Figure 4 and Figure 5 show the PCA projection of the final block’s representations in both the original and approximated models, with a focus on approximating the 11^{th} block. These plots visualize the representations generated using the DiNO-S and DEiT-S pretrained encoders across the MNIST, F-MNIST, CIFAR-10, and CIFAR-100 datasets. For CIFAR-10, having 100 classes, only the overall structure of the representation space is visible, making it difficult to

distinguish individual labels by color. In Figure 4, approximating the final block results in noticeable deviations from the original representations, while in Figure 5, the approximated representation remains similar to the original one. This observation aligns with the results from Figure 3, where approximating the appropriate block can lead to significant changes in representations. For additional visualizations, please refer to Figures 9 to 12.

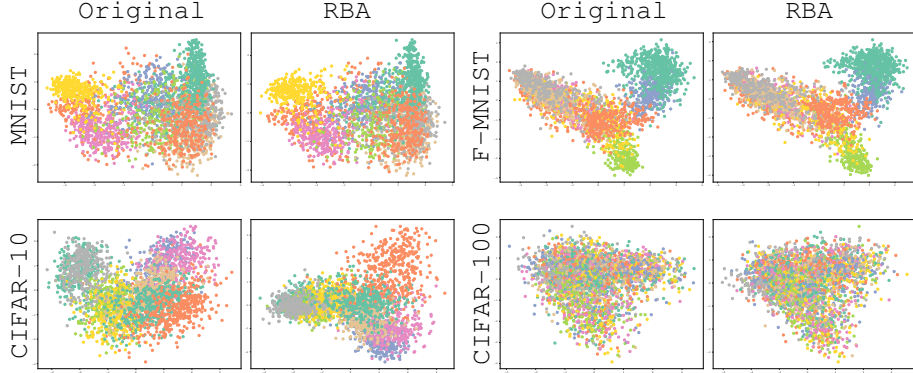


Figure 5: Last Block Approximation. PCA visualization of the final layer representations for both the original model and the model with its last block approximated by the preceding one. The representations are generated using the DEiT-S model across four datasets. The plots highlight that in this model, the representations in the last layer are redundant and can be effectively approximated, offering potential performance improvements while reducing model complexity and parameter count. Note that for CIFAR-100 (bottom right), only the overall structure of the space can be observed, as the 100 classes make it challenging to distinguish labels based on color. For further results approximating other blocks and using other encoders, refer to Figures 9 to 11.

Takeaway. Approximating redundant blocks effectively reduces model parameters and complexity without significantly compromising representation fidelity.

4.3 DOWNSTREAM TASK: CLASSIFICATION

Experimental Setting. We finally conduct image classification using the same datasets and pretrained models described in previous sections, with all models remaining pretrained and frozen. After identifying redundant blocks, the models are restructured accordingly. Approximations between blocks are computed using a shared linear transformation across all tokens, based on a subset of 3,000 training samples. Subsequently, a single linear layer is trained for classification using the Adam optimizer with a learning rate of 0.001 over 5 epochs, three seeds, and a batch size of 256.

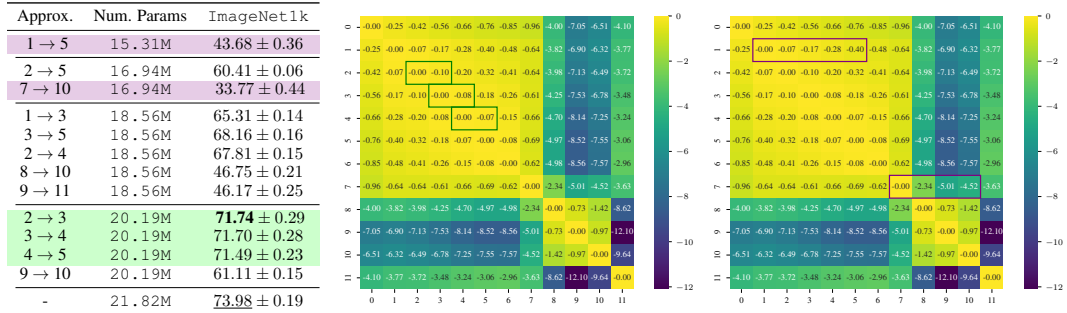


Figure 6: BR and Accuracy Approximation Correlation. (Left) Accuracy performance of the ViT-S encoder with various approximation strategies on ImageNet1k. (Right) The block-by-block BR matrix. Results highlighted in green demonstrate that approximating blocks with high BR values maintains comparable accuracy while reducing parameter count and speeding up computations. Comparatively, results in purple show that approximating four high-BR blocks yields better accuracy than approximating three low-BR blocks, which exhibit lower redundancy.

Table 1: **Image Classification Performance Across Architectures and Seeds.** Classification accuracy scores for ViT-S, DiNO-S and DEiT-S using MNIST, CIFAR-10 and CIFAR-100C, and 3 random seeds. CIFAR-100C refers to CIFAR-100 with the coarse setting (20 labels). The "Approx" column $b_i \rightarrow b_i + n$ specifies the blocks used for approximation, where the first value represents the block whose output is used to approximate the second block's output. The "Num. Blocks" column indicates the total number of remaining blocks after the approximation, and the "Num. Params" column shows the number of model parameters. The proposed method preserves performance while reducing the number of parameters. Please refer to Table 6 for the results on all the models and datasets, as well as Table 7.

Encoder	Approx.	Num. Blocks	Num. Params	Accuracy \uparrow			
				MNIST	CIFAR-10	CIFAR-100C	ImageNet1k
ViT-S	1 \rightarrow 5	8	15.31M	92.11 \pm 0.20	84.93 \pm 0.62	68.47 \pm 0.30	43.68 \pm 0.36
	2 \rightarrow 5	9	16.94M	94.67 \pm 0.12	90.97 \pm 0.30	78.07 \pm 0.38	60.41 \pm 0.06
	7 \rightarrow 10	9	16.94M	94.91 \pm 0.30	85.81 \pm 1.03	71.10 \pm 0.51	33.77 \pm 0.44
	1 \rightarrow 3	10	18.56M	95.67 \pm 0.19	92.09 \pm 0.30	79.68 \pm 0.20	65.31 \pm 0.14
	3 \rightarrow 5	10	18.56M	95.16 \pm 0.08	94.18 \pm 0.11	83.29 \pm 0.47	68.16 \pm 0.16
	2 \rightarrow 4	10	18.56M	95.37 \pm 0.08	93.03 \pm 0.10	81.74 \pm 0.28	67.81 \pm 0.15
	8 \rightarrow 10	10	18.56M	95.27 \pm 0.58	91.56 \pm 0.72	77.73 \pm 0.41	46.75 \pm 0.21
	9 \rightarrow 11	10	18.56M	94.77 \pm 0.10	89.16 \pm 1.10	75.30 \pm 0.44	46.17 \pm 0.25
	2 \rightarrow 3	11	20.19M	95.76 \pm 0.08	94.87 \pm 0.20	85.96 \pm 0.05	71.74 \pm 0.29
	3 \rightarrow 4	11	20.19M	95.70 \pm 0.11	95.10 \pm 0.23	86.00 \pm 0.12	71.70 \pm 0.28
	4 \rightarrow 5	11	20.19M	95.67 \pm 0.17	95.43 \pm 0.25	86.24 \pm 0.21	71.49 \pm 0.23
	9 \rightarrow 10	11	20.19M	95.75 \pm 0.44	94.23 \pm 0.12	82.69 \pm 0.49	61.11 \pm 0.15
	-	12	21.82M	95.95 \pm 0.40	95.87 \pm 0.08	87.60 \pm 0.15	73.98 \pm 0.19
	-	12	21.82M	95.95 \pm 0.40	95.87 \pm 0.08	87.60 \pm 0.15	73.98 \pm 0.19
DiNO-S	1 \rightarrow 5	8	15.55M	95.32 \pm 1.09	79.37 \pm 1.34	60.72 \pm 0.49	19.45 \pm 0.64
	2 \rightarrow 5	9	17.18M	96.04 \pm 0.67	85.58 \pm 0.54	67.89 \pm 0.57	41.39 \pm 0.17
	7 \rightarrow 10	9	17.18M	96.93 \pm 0.45	91.24 \pm 0.13	78.14 \pm 0.14	45.94 \pm 0.40
	1 \rightarrow 3	10	18.80M	96.74 \pm 0.96	91.82 \pm 0.17	78.81 \pm 0.35	57.38 \pm 0.13
	3 \rightarrow 5	10	18.80M	96.93 \pm 0.42	90.90 \pm 0.30	76.12 \pm 0.50	58.01 \pm 0.47
	2 \rightarrow 4	10	18.80M	96.54 \pm 0.55	91.03 \pm 0.75	76.57 \pm 0.25	60.26 \pm 0.26
	8 \rightarrow 10	10	18.80M	97.03 \pm 0.17	93.34 \pm 0.44	82.27 \pm 0.41	53.61 \pm 0.42
	9 \rightarrow 11	10	18.80M	92.46 \pm 1.63	85.65 \pm 0.68	72.44 \pm 1.19	34.50 \pm 0.10
	2 \rightarrow 3	11	20.43M	96.99 \pm 0.70	94.67 \pm 0.20	83.92 \pm 0.49	65.42 \pm 0.25
	3 \rightarrow 4	11	20.43M	97.22 \pm 0.50	94.72 \pm 0.24	83.37 \pm 0.37	65.60 \pm 0.39
	4 \rightarrow 5	11	20.43M	97.33 \pm 0.47	94.64 \pm 0.10	82.81 \pm 0.62	64.58 \pm 0.30
	9 \rightarrow 10	11	20.43M	96.99 \pm 0.97	93.52 \pm 0.48	84.09 \pm 0.52	59.19 \pm 0.10
	-	12	22.06M	<u>96.85</u> \pm 1.04	<u>96.06</u> \pm 0.32	<u>87.62</u> \pm 0.24	<u>67.74</u> \pm 0.23
	-	12	22.06M	<u>96.85</u> \pm 1.04	<u>96.06</u> \pm 0.32	<u>87.62</u> \pm 0.24	<u>67.74</u> \pm 0.23
DEiT-S	1 \rightarrow 5	8	15.31M	93.27 \pm 0.37	78.20 \pm 0.21	59.82 \pm 0.16	43.37 \pm 0.18
	2 \rightarrow 5	9	16.94M	94.99 \pm 0.18	85.27 \pm 0.11	69.95 \pm 0.15	61.67 \pm 0.16
	7 \rightarrow 10	9	16.94M	95.81 \pm 0.23	89.20 \pm 0.34	75.96 \pm 0.20	57.10 \pm 0.22
	1 \rightarrow 3	10	18.56M	95.35 \pm 0.21	85.59 \pm 0.23	70.61 \pm 0.42	66.05 \pm 0.26
	3 \rightarrow 5	10	18.56M	95.86 \pm 0.14	89.12 \pm 0.23	75.84 \pm 0.09	68.51 \pm 0.07
	2 \rightarrow 4	10	18.56M	95.68 \pm 0.11	88.76 \pm 0.08	75.83 \pm 0.38	69.96 \pm 0.12
	8 \rightarrow 10	10	18.56M	95.87 \pm 0.27	90.62 \pm 0.09	78.25 \pm 0.52	66.29 \pm 0.23
	9 \rightarrow 11	10	18.56M	95.64 \pm 0.13	91.09 \pm 0.21	79.30 \pm 0.58	69.63 \pm 0.24
	2 \rightarrow 3	11	20.19M	95.99 \pm 0.19	90.13 \pm 0.23	78.11 \pm 0.23	73.17 \pm 0.19
	3 \rightarrow 4	11	20.19M	96.05 \pm 0.09	90.33 \pm 0.26	78.70 \pm 0.39	72.75 \pm 0.09
	4 \rightarrow 5	11	20.19M	95.88 \pm 0.18	90.26 \pm 0.17	78.12 \pm 0.20	72.28 \pm 0.17
	9 \rightarrow 10	11	20.19M	95.96 \pm 0.24	91.08 \pm 0.25	79.33 \pm 0.34	72.00 \pm 0.09
	-	12	21.82M	<u>96.03</u> \pm 0.24	<u>90.83</u> \pm 0.11	<u>79.06</u> \pm 0.30	<u>73.95</u> \pm 0.09
	-	12	21.82M	<u>96.03</u> \pm 0.24	<u>90.83</u> \pm 0.11	<u>79.06</u> \pm 0.30	<u>73.95</u> \pm 0.09

Results and Analysis. As illustrated in Table 1, employing RBA allows for reducing model size while maintaining, and in some cases even improving, performance. Notably, as discussed in Section 4.2 and illustrated in Figure 3 and Figure 5, using DEiT-S to approximate the last blocks yields better results, even when approximating multiple blocks such as 9 \rightarrow 11 or 8 \rightarrow 10. In contrast, with ViT-S, the same approximations result in a slight decrease in performance. Moreover, in Figure 6, we illustrate the correlation between the redundancies identified by the BR metric and the results obtained when approximating the identified redundant representations using the ViT-S and the ImageNet1k dataset. As shown in the leftmost correlation matrix and highlighted in green in the table, approximating redundant blocks yields comparable results while reducing both the number of parameters and computational cost. Additionally, the rightmost correlation matrix, along with

the results highlighted in violet in the table, demonstrates that approximating four redundant blocks yields better results than approximating three non-redundant blocks. Overall, performance remains similar or improved, demonstrating that a simple linear transformation is sufficient to approximate different blocks of a NN, significantly reducing the number of parameters and model complexity. It’s important to note that this transformation is uniformly applied to all tokens, further optimizing the process, with no additional training or fine-tuning required afterward. Additional results on classification performance can be found in Table 6.

Table 2: Image Classification Performance: RBA vs. Skip Across Seeds. Accuracy scores for ViT-S on CIFAR-10 and CIFAR-100F are reported using 3 different seeds. The "Approx." column $b_i \rightarrow b_i + n$ specifies the blocks being approximated, where the first value represents the block whose output is used to approximate the second block’s output. The "Skip" column represents the operation of skipping a block instead of approximating it, while the "Num. Blocks" column shows the total number of remaining blocks. Results demonstrate that approximating outperforms skipping in all cases. Refer to Table 8 for results on the other datasets.

Encoder	Approx.	Num. Blocks	Skip Accuracy \uparrow		Approximate Accuracy \uparrow	
			CIFAR-10	CIFAR-100F	CIFAR-10	CIFAR-100F
ViT-S	1 \rightarrow 5	8	58.08 \pm 0.44	32.68 \pm 0.70	84.93 \pm 0.62	58.98 \pm 0.19
	2 \rightarrow 5	9	64.43 \pm 2.00	41.78 \pm 0.45	90.97 \pm 0.30	69.85 \pm 0.18
	7 \rightarrow 10	9	73.94 \pm 0.34	45.00 \pm 0.31	85.81 \pm 1.03	60.33 \pm 0.85
	1 \rightarrow 3	10	66.27 \pm 0.76	42.76 \pm 0.75	92.09 \pm 0.30	72.13 \pm 0.37
	3 \rightarrow 5	10	74.79 \pm 1.56	54.62 \pm 0.52	94.18 \pm 0.11	76.45 \pm 0.23
	2 \rightarrow 4	10	71.56 \pm 1.62	50.19 \pm 0.38	93.03 \pm 0.10	74.65 \pm 0.59
	8 \rightarrow 10	10	85.74 \pm 0.32	63.79 \pm 0.66	91.56 \pm 0.72	69.35 \pm 0.22
	9 \rightarrow 11	10	89.65 \pm 0.52	70.75 \pm 0.39	89.16 \pm 1.10	68.25 \pm 0.57
	0 \rightarrow 1	11	70.90 \pm 0.09	47.54 \pm 0.37	93.67 \pm 0.27	76.53 \pm 0.33
	1 \rightarrow 2	11	83.21 \pm 0.52	62.23 \pm 0.21	93.81 \pm 0.18	77.21 \pm 0.12
	2 \rightarrow 3	11	81.24 \pm 0.48	60.22 \pm 0.75	94.87 \pm 0.20	79.16 \pm 0.43
	3 \rightarrow 4	11	88.25 \pm 0.23	69.79 \pm 0.02	95.10 \pm 0.23	79.57 \pm 0.43
	4 \rightarrow 5	11	86.23 \pm 0.63	66.69 \pm 0.48	95.43 \pm 0.25	79.86 \pm 0.20
	5 \rightarrow 6	11	83.42 \pm 0.52	61.96 \pm 0.55	95.09 \pm 0.21	79.48 \pm 0.46
	6 \rightarrow 7	11	87.57 \pm 0.24	68.70 \pm 0.31	94.73 \pm 0.13	78.27 \pm 0.12
	7 \rightarrow 8	11	88.70 \pm 0.46	69.33 \pm 0.39	94.77 \pm 0.17	78.18 \pm 0.17
	8 \rightarrow 9	11	89.98 \pm 0.48	71.80 \pm 0.22	94.04 \pm 0.29	77.88 \pm 0.20
	9 \rightarrow 10	11	93.40 \pm 0.32	76.32 \pm 0.30	94.23 \pm 0.12	76.69 \pm 0.36
	10 \rightarrow 11	11	93.77 \pm 0.69	78.68 \pm 0.29	93.68 \pm 0.65	77.47 \pm 0.17
	-	12	95.87 \pm 0.08	81.29 \pm 0.20	95.87 \pm 0.08	81.52 \pm 0.15

Ablation Analysis. Additionally, we evaluated the model’s performance when completely skipping blocks instead of approximating them. As for the previous setting, after performing the desired skips, the network is not trained or fine-tuned. The results in Table 2 show the accuracy scores for ViT-S on CIFAR-10 and CIFAR-100F, where the "Skip" column represents the operation of skipping a block entirely rather than applying an approximation. The findings consistently demonstrate that approximating blocks significantly outperforms skipping them in all cases. This underscores the effectiveness of RBA in preserving model performance while reducing complexity. Please refer to Table 8 for results on other datasets.

Generalization. Finally, we evaluated the model’s performance in approximating representations based on a transformation calculated on a different dataset using the same architecture. As in the previous setting, after applying the desired skips, the network is neither trained nor fine-tuned. The results in Table 3 show the accuracy scores for ViT-S and DiNO-S on MNIST, CIFAR-10, and CIFAR-100F, where the "Fit On" column indicates the dataset used to calculate the transformation. With the exception of MNIST, which might be too basic to generalize effectively, the findings consistently demonstrate that it is possible to leverage a simple linear transformation that is not only shared across all tokens but also across different datasets. Additional results can be found in Table 9.

Takeaway. Redundant Block Approximation preserves essential representational features while maintaining the model’s structural integrity, even when simplifying its architecture, whereas just skipping blocks could lead to performance degradation.

Table 3: **Generalization Results.** Classification accuracy scores when approximating using a transformation calculated on other datasets for ViT-S and DiNO-S using MNIST, CIFAR-10, CIFAR-100C and CIFAR-100F. CIFAR-100C refers to CIFAR-100 with the coarse setting (20 labels), while CIFAR-100F with the fine setting (100 labels). The "Approx" column $b_i \rightarrow b_i + n$ specifies the blocks used for approximation, where the first value represents the block whose output is used to approximate the second block's output. The "Fit On" column indicates the dataset on which is calculated the linear transformation. Please refer to Table 9 for complete results.

Encoder	Approx.	Fit On	Accuracy \uparrow			
			MNIST	CIFAR-10	CIFAR-100C	CIFAR-100F
ViT-S	2 \rightarrow 3	MNIST	94.11	57.13	41.89	28.50
		CIFAR-10	89.58	95.08	85.32	77.92
		CIFAR-100	89.63	95.00	85.50	77.74
	3 \rightarrow 4	MNIST	93.52	10.36	8.97	3.09
		CIFAR-10	88.02	95.18	86.14	78.52
		CIFAR-100	88.21	94.82	85.92	78.09
	4 \rightarrow 5	MNIST	93.96	38.40	25.56	16.52
		CIFAR-10	78.36	95.31	85.84	78.20
		CIFAR-100	80.11	94.98	86.01	78.14
	1 \rightarrow 3	MNIST	92.79	16.17	11.09	3.84
		CIFAR-10	80.41	90.63	75.59	65.98
		CIFAR-100	81.24	89.98	76.27	66.26
	3 \rightarrow 5	MNIST	88.22	15.17	8.52	2.03
		CIFAR-10	61.68	93.57	80.24	71.76
		CIFAR-100	64.18	92.77	80.56	72.43
DiNO-S	2 \rightarrow 3	MNIST	93.04	58.24	37.95	27.62
		CIFAR-10	86.16	94.11	82.37	75.26
		CIFAR-100	86.39	93.78	82.28	75.29
	3 \rightarrow 4	MNIST	92.33	62.78	38.18	27.52
		CIFAR-10	84.70	94.37	81.93	74.69
		CIFAR-100	83.72	94.10	82.02	74.59
	4 \rightarrow 5	MNIST	91.64	57.39	36.97	26.02
		CIFAR-10	70.87	93.65	80.38	73.84
		CIFAR-100	71.51	92.98	79.96	73.54
	1 \rightarrow 3	MNIST	90.60	22.30	11.76	5.47
		CIFAR-10	78.51	89.72	74.58	65.04
		CIFAR-100	79.80	89.28	74.75	64.92
	3 \rightarrow 5	MNIST	87.54	24.55	11.93	6.67
		CIFAR-10	63.66	87.17	66.16	58.36
		CIFAR-100	64.26	84.40	66.43	58.51

5 CONCLUSION

In this paper, we introduced a novel framework for approximating redundant representations in transformer-based foundation models and proposed a simple yet effective metric to identify such redundancies. By leveraging a simple linear transformation, shared across all tokens, between consecutive and non-consecutive blocks output, we demonstrated that it is possible to significantly reduce model parameters and complexity without sacrificing performance, and in some cases even improving it. Our approach provides an efficient way to optimize model architecture, maintaining essential representation fidelity while streamlining the network for downstream tasks.

Limitations and Future Works. While our framework shows promising results, it has been primarily tested on transformer-based architectures. We leave to future work to explore the application of our framework across different modalities (e.g., text), architectures (e.g., ResNets and AutoEncoders), and downstream tasks (e.g., reconstruction). Additionally, we plan to enhance the representation analysis by incorporating topological metrics, which could provide a different perspective on structural similarities between representations. This alternative viewpoint may uncover new insights into redundancy patterns and further refine our approach. By expanding the framework's scope, we aim to validate its versatility and continue optimizing model efficiency across a broader set of architectures and tasks, advancing its practical applicability in diverse settings.

REFERENCES

- Shipeng Bai, Jun Chen, Xintian Shen, Yixuan Qian, and Yong Liu. Unified data-free compression: Pruning and quantization without fine-tuning. In *Proceedings of the IEEE/CVF International Conference on Computer Vision*, pp. 5876–5885, 2023.
- Rubén Ballester, Carles Casacuberta, and Sergio Escalera. Topological data analysis for neural network analysis: A comprehensive survey. *arXiv preprint arXiv:2312.05840*, December 2023.
- Serguei Barannikov, Ilya Trofimov, Nikita Balabin, and Evgeny Burnaev. Representation topology divergence: A method for comparing neural network representations. *arXiv preprint arXiv:2201.00058*, 2021.
- Irene Cannistraci, Luca Moschella, Valentino Maiorca, Marco Fumero, Antonio Norelli, and Emanuele Rodolà. Bootstrapping parallel anchors for relative representations, 2023. URL <https://openreview.net/forum?id=VBuUL2IWlq>.
- Irene Cannistraci, Luca Moschella, Marco Fumero, Valentino Maiorca, and Emanuele Rodolà. From bricks to bridges: Product of invariances to enhance latent space communication. In *The Twelfth International Conference on Learning Representations*, 2024. URL <https://openreview.net/forum?id=vngVydDWft>.
- Donato Crisostomi, Irene Cannistraci, Luca Moschella, Pietro Barbiero, Marco Ciccone, Pietro Lio, and Emanuele Rodolà. From charts to atlas: Merging latent spaces into one. In *NeurIPS 2023 Workshop on Symmetry and Geometry in Neural Representations*, 2023. URL <https://openreview.net/forum?id=ZFu7CPTznY>.
- MohammadReza Davari, Stefan Horoi, Amine Natic, Guillaume Lajoie, Guy Wolf, and Eugene Belilovsky. Reliability of cka as a similarity measure in deep learning. *arXiv preprint arXiv:2210.16156*, 2022.
- Li Deng. The mnist database of handwritten digit images for machine learning research. *IEEE Signal Processing Magazine*, 29(6):141–142, 2012.
- Alexey Dosovitskiy, Lucas Beyer, Alexander Kolesnikov, Dirk Weissenborn, Xiaohua Zhai, Thomas Unterthiner, Mostafa Dehghani, Matthias Minderer, Georg Heigold, Sylvain Gelly, Jakob Uszkoreit, and Neil Houlsby. An image is worth 16x16 words: Transformers for image recognition at scale. In *9th International Conference on Learning Representations, ICLR 2021, Virtual Event, Austria, May 3-7, 2021*. OpenReview.net, 2021. URL <https://openreview.net/forum?id=YicbFdNTTy>.
- Marco Fumero, Marco Pegoraro, Valentino Maiorca, Francesco Locatello, and Emanuele Rodolà. Latent functional maps. In *Proc. NeurIPS*, 2024.
- Harold Hotelling. Relations between two sets of variates. *Breakthroughs in statistics: methodology and distribution*, pp. 162–190, 1992.
- Max Klabunde, Tobias Schumacher, Markus Strohmaier, and Florian Lemmerich. Similarity of neural network models: A survey of functional and representational measures. *arXiv preprint arXiv:2305.06329*, 2023.
- Simon Kornblith, Mohammad Norouzi, Honglak Lee, and Geoffrey Hinton. Similarity of neural network representations revisited. In *International Conference on Machine Learning*, pp. 3519–3529. PMLR, 2019.
- Alex Krizhevsky, Geoffrey Hinton, et al. Learning multiple layers of features from tiny images. Toronto, ON, Canada, 2009.
- Ruslan Kuprieiev, skshetry, Dmitry Petrov, Paweł Redzyński, Peter Rowlands, Casper da Costa-Luis, Alexander Schepanovski, Ivan Shcheklein, Batuhan Taskaya, Gao, Jorge Orpinel, David de la Iglesia Castro, Fábio Santos, Aman Sharma, Dave Berenbaum, Zhanibek, Dani Hodovic, danielle, Nikita Kodenko, Andrew Grigorev, Earl, Nabanita Dash, George Vyshnya, Ronan Lamy, maykulkarni, Max Hora, Vera, and Sanidhya Mangal. Dvc: Data version control - git for data & models, 2022. URL <https://doi.org/10.5281/zenodo.7083378>.

- Henry Kvinge, Grayson Jorgenson, Davis Brown, Charles Godfrey, and Tegan Emerson. Internal representations of vision models through the lens of frames on data manifolds. In *NeurIPS 2023 Workshop on Symmetry and Geometry in Neural Representations*, 2022.
- Zorah Löhner and Michael Moeller. On the direct alignment of latent spaces. In Marco Fumero, Emanuele Rodolà, Clementine Domine, Francesco Locatello, Karolina Dziugaite, and Caron Mathilde (eds.), *Proceedings of UniReps: the First Workshop on Unifying Representations in Neural Models*, volume 243 of *Proceedings of Machine Learning Research*, pp. 158–169. PMLR, 15 Dec 2024. URL <https://proceedings.mlr.press/v243/lahner24a.html>.
- Zhu Liao, Victor Quétu, Van-Tam Nguyen, and Enzo Tartaglione. Can unstructured pruning reduce the depth in deep neural networks? In *Proceedings of the IEEE/CVF International Conference on Computer Vision*, pp. 1402–1406, 2023.
- Xinyin Ma, Gongfan Fang, and Xinchao Wang. Llm-pruner: On the structural pruning of large language models. *Advances in neural information processing systems*, 36:21702–21720, 2023.
- Valentino Maiorca, Luca Moschella, Antonio Norelli, Marco Fumero, Francesco Locatello, and Emanuele Rodolà. Latent space translation via semantic alignment. *Advances in Neural Information Processing Systems*, 36, 2024.
- Ari Morcos, Maithra Raghu, and Samy Bengio. Insights on representational similarity in neural networks with canonical correlation. *Advances in Neural Information Processing Systems*, 31, 2018.
- Luca Moschella, Valentino Maiorca, Marco Fumero, Antonio Norelli, Francesco Locatello, and Emanuele Rodolà. Relative representations enable zero-shot latent space communication. In *Proc. ICLR*, 2023.
- Thao Nguyen, Maithra Raghu, and Simon Kornblith. Do wide and deep networks learn the same things? uncovering how neural network representations vary with width and depth. *arXiv preprint arXiv:2010.15327*, 2020.
- Antonio Norelli, Marco Fumero, Valentino Maiorca, Luca Moschella, Emanuele Rodola, and Francesco Locatello. Asif: Coupled data turns unimodal models to multimodal without training. *Advances in Neural Information Processing Systems*, 36:15303–15319, 2023.
- Maxime Oquab, Timothée Darcet, Théo Moutakanni, Huy Vo, Marc Szafraniec, Vasil Khalidov, Pierre Fernandez, Daniel Haziza, Francisco Massa, Alaaeldin El-Nouby, et al. Dinov2: Learning robust visual features without supervision. *arXiv preprint arXiv:2304.07193*, 2023.
- Maithra Raghu, Justin Gilmer, Jason Yosinski, and Jascha Sohl-Dickstein. Svcca: Singular vector canonical correlation analysis for deep learning dynamics and interpretability. *Advances in neural information processing systems*, 30, 2017.
- Antonio Pio Ricciardi, Valentino Maiorca, Luca Moschella, and Emanuele Rodolà. Zero-shot stitching in reinforcement learning using relative representations. In *Sixteenth European Workshop on Reinforcement Learning*, 2023. URL <https://openreview.net/forum?id=4tcXsImfsS1>.
- Hassan Sajjad, Fahim Dalvi, Nadir Durrani, and Preslav Nakov. On the effect of dropping layers of pre-trained transformer models. *Computer Speech & Language*, 77:101429, 2023.
- Shengkun Tang, Yaqing Wang, Zhenglun Kong, Tianchi Zhang, Yao Li, Caiwen Ding, Yanzhi Wang, Yi Liang, and Dongkuan Xu. You need multiple exiting: Dynamic early exiting for accelerating unified vision language model. In *Proceedings of the IEEE/CVF Conference on Computer Vision and Pattern Recognition*, pp. 10781–10791, 2023.
- Hugo Touvron, Matthieu Cord, Matthijs Douze, Francisco Massa, Alexandre Sablayrolles, and Hervé Jégou. Training data-efficient image transformers & distillation through attention. *arxiv preprint arXiv:2012.12877*, 2(3), 2020.
- Lucrezia Valeriani, Diego Doimo, Francesca Cuturello, Alessandro Laio, Alessio Ansuini, and Alberto Cazzaniga. The geometry of hidden representations of large transformer models. *Advances in Neural Information Processing Systems*, 36, 2024.

- Shashanka Venkataramanan, Amir Ghodrati, Yuki M Asano, Fatih Porikli, and Amir Habibian. Skip-attention: Improving vision transformers by paying less attention. In *The Twelfth International Conference on Learning Representations*, 2024. URL <https://openreview.net/forum?id=vI95kcLAoU>.
- Han Xiao, Kashif Rasul, and Roland Vollgraf. Fashion-mnist: a novel image dataset for benchmarking machine learning algorithms. *arXiv preprint arXiv:1708.07747*, 2017.
- Ji Xin, Raphael Tang, Jaejun Lee, Yaoliang Yu, and Jimmy Lin. Deebert: Dynamic early exiting for accelerating bert inference. *arXiv preprint arXiv:2004.12993*, 2020.
- Fang Yu, Kun Huang, Meng Wang, Yuan Cheng, Wei Chu, and Li Cui. Width & depth pruning for vision transformers. In *Proc. AAAI*, 2022.
- Hanxiao Zhang, Yifan Zhou, and Guo-Hua Wang. Dense vision transformer compression with few samples. In *Proceedings of the IEEE/CVF Conference on Computer Vision and Pattern Recognition (CVPR)*, pp. 15825–15834, June 2024.
- Minjia Zhang and Yuxiong He. Accelerating training of transformer-based language models with progressive layer dropping. *Advances in neural information processing systems*, 33:14011–14023, 2020.
- Wangchunshu Zhou, Canwen Xu, Tao Ge, Julian McAuley, Ke Xu, and Furu Wei. Bert loses patience: Fast and robust inference with early exit. *Advances in Neural Information Processing Systems*, 33: 18330–18341, 2020.

A APPENDIX

A.1 REPRODUCIBILITY STATEMENT

In Section 3, we provide a detailed description of the proposed framework and the experimental settings for the various scenarios. In the following sections, we present all implementation details that are not described in the main manuscript. Additionally, we will release a modular PyTorch implementation.

A.2 IMPLEMENTATION DETAILS

This section details the experiments conducted in Section 4. Table 4 contains the full list of the pretrained models, while Table 5 contains dataset information.

Table 4: **Pretrained models details.** Details of the pretrained feature extractors with their HuggingFace key, their alias, and their latent space dimensionality.

Modality	HuggingFace Model Name	Alias	Enc. Dim
Vision	WinKawaks/vit-small-patch16-224	ViT-S (Dosovitskiy et al., 2021)	384
	google/vit-base-patch16-224	ViT-B (Dosovitskiy et al., 2021)	768
	facebook/dinov2-small	DiNO-S (Oquab et al., 2023)	384
	facebook/dinov2-base	DiNO-B (Oquab et al., 2023)	768
	facebook/deit-small-patch16-224	DEiT-S (Touvron et al., 2020)	384

Table 5: **Dataset details.** Details of the HuggingFace datasets used in the classification and reconstruction experiments, with the associated number of classes.

Modality	Name	Alias	Number of Classes
Image	MNIST (Deng, 2012)	MNIST	10
	Fasion-MNIST (Xiao et al., 2017)	F-MNIST	10
	CIFAR-10 (Krizhevsky et al., 2009)	CIFAR-10	10
	CIFAR-100 (coarse) (Krizhevsky et al., 2009)	CIFAR-100C	20
	CIFAR-100 (fine) (Krizhevsky et al., 2009)	CIFAR-100F	100

A.2.1 TOOLS & TECHNOLOGIES

All the experiments presented in this work employ the following tools:

- *PyTorch Lightning*, to ensure reproducible results while also getting a clean and modular codebase;
- *NN-Template GrokAI (2021)*, to easily bootstrap the project and enforce best practices;
- *Transformers by HuggingFace*, to get ready-to-use transformers for both text and images;
- *Datasets by HuggingFace*, to access most of the datasets;
- *DVC* (Kupriev et al., 2022), for data versioning;

A.3 ADDITIONAL EXPERIMENTS

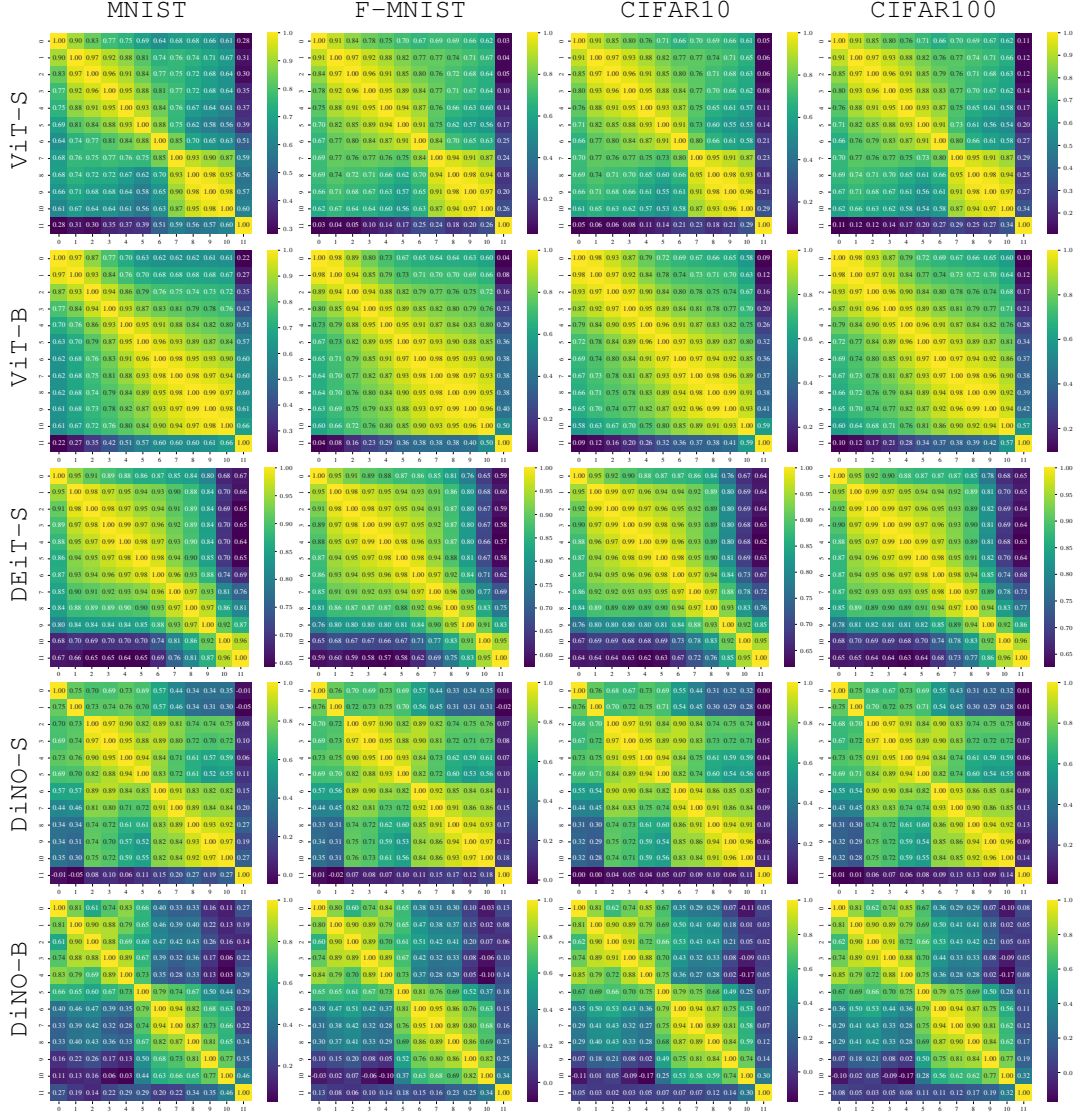


Figure 7: **Representation Similarities.** Cosine similarity matrices illustrating the internal block-by-block similarities in ViT-S, ViT-B, DEiT-S, DiNO-S and DiNO-B, and DEiT-S models across four datasets: MNIST, F-MNIST, CIFAR-10, and CIFAR-100. Each heatmap quantifies the similarity between the internal representations of different blocks using the [CLS] token, providing insights into redundancy in foundation pretrained models. The matrices reveal that the similarity structure between computational blocks is predominantly influenced by the model architecture itself rather than the specific dataset.

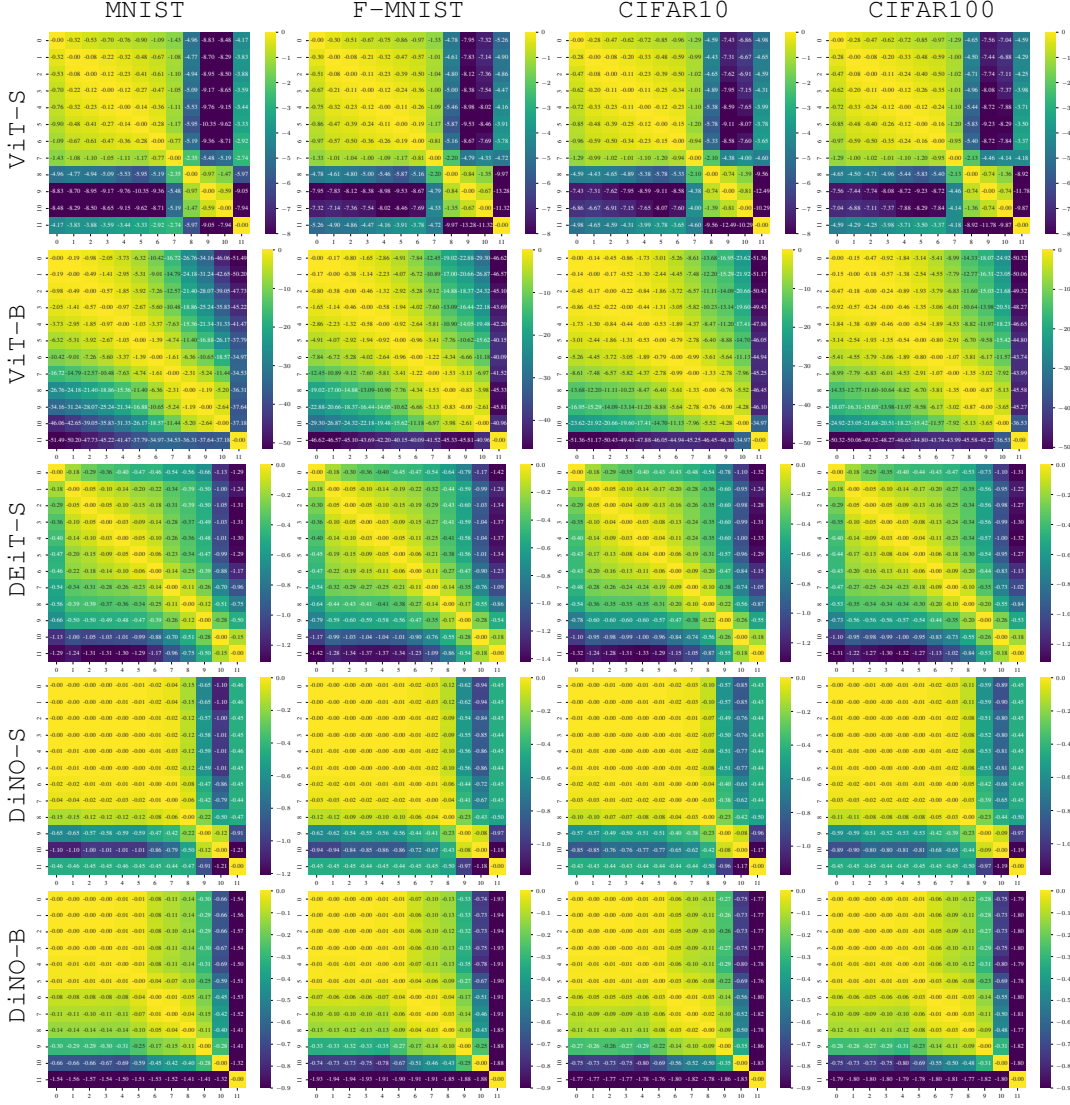


Figure 8: Representation Redundancies. BR matrices illustrating the internal block-by-block redundancies in ViT-S, ViT-B, DEiT-S, DiNO-S and DiNO-B, and DEiT-S models across four datasets: MNIST, F-MNIST, CIFAR-10, and CIFAR-100. Each heatmap quantifies the BR metric between the internal representations of different blocks using the [CLS] token, providing insights into redundancy in foundation pretrained models. The matrices reveal that the similarity structure between computational blocks is predominantly influenced by the model architecture itself rather than the specific dataset.

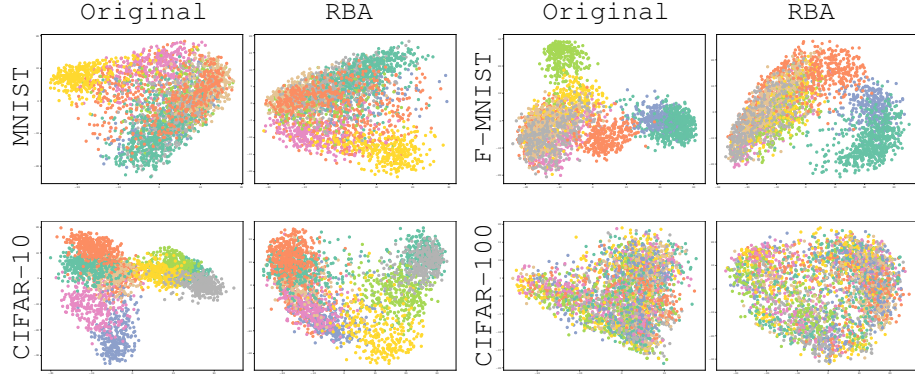


Figure 9: **Last Block Approximation.** PCA visualization of the final layer representations for both the original model and the model with its second block approximated by the preceding one. The representations are generated using the DiNO-S model across four datasets. Note that for CIFAR-100 (bottom right), only the overall structure of the space can be observed, as the 100 classes make it challenging to distinguish labels based on color

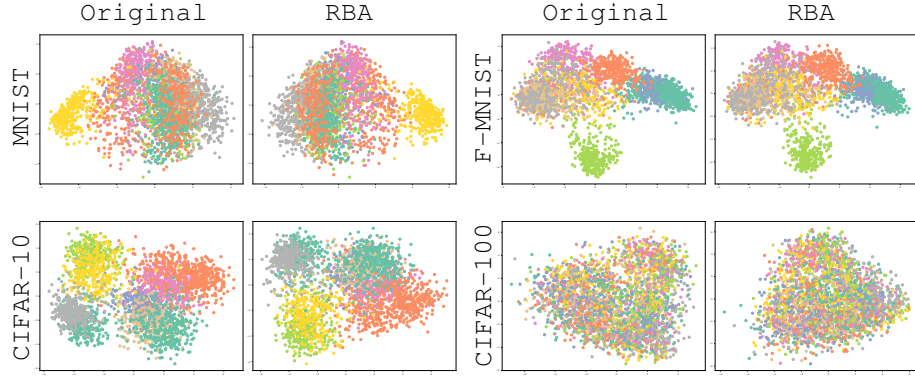


Figure 10: **Last Block Approximation.** PCA visualization of the last layer representations for both the original model and the model with its second block approximated using the previous one. Representations refer to the using ViT-S model across four datasets.

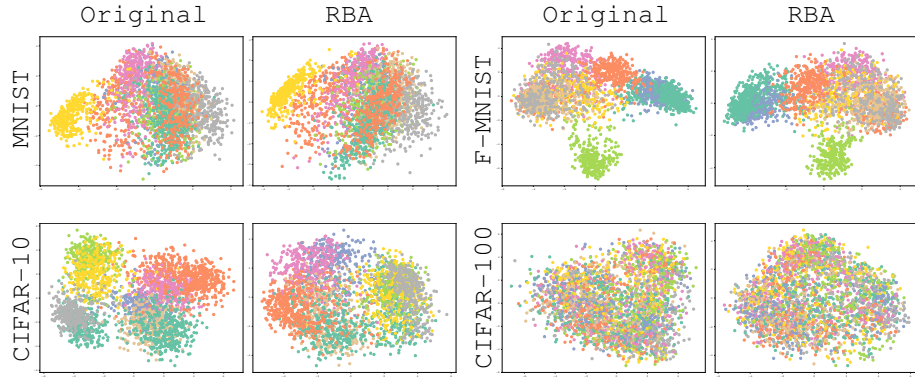


Figure 11: **Last Block Approximation.** PCA visualization of the last layer representations for both the original model and the model with its last block approximated from the previous one. Representations refer to the using ViT-S model across four datasets.

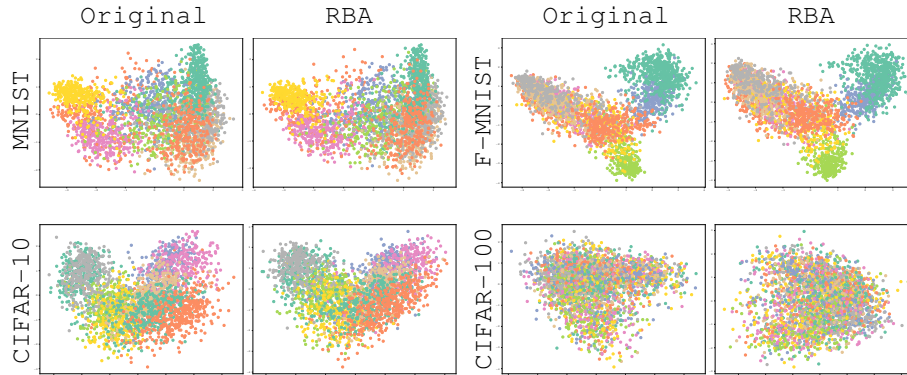


Figure 12: **Last Block Approximation.** PCA visualization of the last layer representations for both the original model and the model with its last block approximated from the previous one. Representations refer to the using DEiT-S model across four datasets.

Table 6: **Image Classification Performance Across Architectures and Seeds.** Accuracy scores are reported for different pretrained models, random seeds, and datasets. CIFAR-100C refers to CIFAR-100 with the coarse setting (20 labels), while CIFAR-100F refers to the fine setting (100 labels). The "Approx" column $b_i \rightarrow b_i + n$ specifies the blocks used for approximation, where the first value represents the block whose output is used to approximate the second block's output. The "Num. Blocks" column indicates the total number of remaining blocks after the approximation, and the "Num. Params" column shows the number of model parameters. The proposed method preserves performance while reducing the number of parameters.

Encoder	Approx.	Num. Blocks	Num. Params	Accuracy \uparrow				
				MNIST	F-MNIST	CIFAR-10	CIFAR-100C	CIFAR-100F
ViT-S	1 \rightarrow 5	8	15.31M	92.11 \pm 0.20	86.36 \pm 1.00	84.93 \pm 0.62	68.47 \pm 0.30	58.96 \pm 0.20
	2 \rightarrow 5	9	16.94M	94.67 \pm 0.12	87.82 \pm 0.92	90.97 \pm 0.30	78.07 \pm 0.38	69.83 \pm 0.19
	7 \rightarrow 10	9	16.94M	94.91 \pm 0.30	88.00 \pm 0.78	85.81 \pm 1.03	71.10 \pm 0.51	60.18 \pm 0.93
	1 \rightarrow 3	10	18.56M	95.67 \pm 0.19	87.43 \pm 0.63	92.09 \pm 0.30	79.68 \pm 0.20	72.12 \pm 0.27
	3 \rightarrow 5	10	18.56M	95.16 \pm 0.08	88.38 \pm 0.80	94.18 \pm 0.11	83.29 \pm 0.47	76.46 \pm 0.23
	2 \rightarrow 4	10	18.56M	95.37 \pm 0.08	88.08 \pm 1.08	93.03 \pm 0.10	81.74 \pm 0.28	74.69 \pm 0.60
	8 \rightarrow 10	10	18.56M	95.27 \pm 0.58	88.56 \pm 0.95	91.56 \pm 0.72	77.73 \pm 0.41	69.36 \pm 0.22
	9 \rightarrow 11	10	18.56M	94.77 \pm 0.10	88.23 \pm 0.42	89.16 \pm 1.10	75.30 \pm 0.44	68.19 \pm 0.59
	2 \rightarrow 3	11	20.19M	95.76 \pm 0.08	88.67 \pm 0.63	94.87 \pm 0.20	85.96 \pm 0.05	79.21 \pm 0.45
	3 \rightarrow 4	11	20.19M	95.70 \pm 0.11	88.35 \pm 1.00	95.10 \pm 0.23	86.00 \pm 0.12	79.57 \pm 0.43
	4 \rightarrow 5	11	20.19M	95.67 \pm 0.17	89.11 \pm 0.45	95.43 \pm 0.25	86.24 \pm 0.21	79.87 \pm 0.20
	9 \rightarrow 10	11	20.19M	95.75 \pm 0.44	88.85 \pm 0.90	94.23 \pm 0.12	82.69 \pm 0.49	76.65 \pm 0.37
	-	12	21.82M	<u>95.95</u> \pm 0.40	<u>89.01</u> \pm 0.63	<u>95.87</u> \pm 0.08	<u>87.60</u> \pm 0.15	<u>81.44</u> \pm 0.19
	1 \rightarrow 5	8	15.55M	95.32 \pm 1.09	87.43 \pm 0.78	79.37 \pm 1.34	60.72 \pm 0.49	51.72 \pm 0.44
	2 \rightarrow 5	9	17.18M	96.04 \pm 0.67	88.43 \pm 0.65	85.58 \pm 0.54	67.89 \pm 0.57	60.21 \pm 0.60
DiNO-S	7 \rightarrow 10	9	17.18M	96.93 \pm 0.45	87.47 \pm 0.74	91.24 \pm 0.13	78.14 \pm 0.14	70.46 \pm 0.23
	1 \rightarrow 3	10	18.80M	96.74 \pm 0.96	87.60 \pm 1.68	91.82 \pm 0.17	78.81 \pm 0.35	71.79 \pm 0.22
	3 \rightarrow 5	10	18.80M	96.93 \pm 0.42	88.54 \pm 0.21	90.90 \pm 0.30	76.12 \pm 0.50	69.16 \pm 0.74
	2 \rightarrow 4	10	18.80M	96.54 \pm 0.55	87.63 \pm 1.29	91.03 \pm 0.75	76.57 \pm 0.25	69.82 \pm 0.60
	8 \rightarrow 10	10	18.80M	97.03 \pm 0.17	87.77 \pm 1.38	93.34 \pm 0.44	82.27 \pm 0.41	75.02 \pm 1.12
	9 \rightarrow 11	10	18.80M	92.46 \pm 1.63	82.68 \pm 0.92	85.65 \pm 0.68	72.44 \pm 1.19	60.73 \pm 0.62
	2 \rightarrow 3	11	20.43M	96.99 \pm 0.70	88.62 \pm 0.54	94.67 \pm 0.20	83.92 \pm 0.49	78.34 \pm 0.30
	3 \rightarrow 4	11	20.43M	97.22 \pm 0.50	88.06 \pm 1.01	94.72 \pm 0.24	83.37 \pm 0.37	78.14 \pm 0.20
	4 \rightarrow 5	11	20.43M	97.33 \pm 0.47	88.67 \pm 1.36	94.64 \pm 0.10	82.81 \pm 0.62	76.99 \pm 0.37
	9 \rightarrow 10	11	20.43M	96.99 \pm 0.97	88.41 \pm 0.33	93.52 \pm 0.48	84.09 \pm 0.52	77.54 \pm 0.89
	-	12	22.06M	<u>96.85</u> \pm 1.04	<u>88.17</u> \pm 0.64	<u>96.06</u> \pm 0.32	<u>87.62</u> \pm 0.24	<u>82.09</u> \pm 0.23
	1 \rightarrow 5	8	15.31M	93.27 \pm 0.37	85.76 \pm 0.30	78.20 \pm 0.21	59.82 \pm 0.16	50.72 \pm 0.31
	2 \rightarrow 5	9	16.94M	94.99 \pm 0.18	87.41 \pm 0.27	85.27 \pm 0.11	69.95 \pm 0.15	61.25 \pm 0.29
	7 \rightarrow 10	9	16.94M	95.81 \pm 0.23	87.82 \pm 0.43	89.20 \pm 0.34	75.96 \pm 0.20	69.22 \pm 0.21
	1 \rightarrow 3	10	18.56M	95.35 \pm 0.21	87.11 \pm 0.32	85.59 \pm 0.23	70.61 \pm 0.42	61.74 \pm 0.07
DEiT-S	3 \rightarrow 5	10	18.56M	95.86 \pm 0.14	87.79 \pm 0.51	89.12 \pm 0.23	75.84 \pm 0.09	67.25 \pm 0.20
	2 \rightarrow 4	10	18.56M	95.68 \pm 0.11	87.96 \pm 0.39	88.76 \pm 0.08	75.83 \pm 0.38	67.01 \pm 0.31
	8 \rightarrow 10	10	18.56M	95.87 \pm 0.27	88.05 \pm 0.37	90.62 \pm 0.09	78.25 \pm 0.52	71.03 \pm 0.31
	9 \rightarrow 11	10	18.56M	95.64 \pm 0.13	88.26 \pm 0.11	91.09 \pm 0.21	79.30 \pm 0.58	71.77 \pm 0.33
	2 \rightarrow 3	11	20.19M	95.99 \pm 0.19	87.85 \pm 0.33	90.13 \pm 0.23	78.11 \pm 0.23	70.13 \pm 0.09
	3 \rightarrow 4	11	20.19M	96.05 \pm 0.09	87.97 \pm 0.14	90.33 \pm 0.26	78.70 \pm 0.39	70.40 \pm 0.21
	4 \rightarrow 5	11	20.19M	95.88 \pm 0.18	88.04 \pm 0.31	90.26 \pm 0.17	78.12 \pm 0.20	69.66 \pm 0.38
	9 \rightarrow 10	11	20.19M	95.96 \pm 0.24	88.09 \pm 0.17	91.08 \pm 0.25	79.33 \pm 0.34	71.62 \pm 0.10
	-	12	21.82M	<u>96.03</u> \pm 0.24	<u>87.86</u> \pm 0.25	<u>90.83</u> \pm 0.11	<u>79.06</u> \pm 0.30	<u>71.25</u> \pm 0.18

Table 7: **Image Classification Performance Across Seeds.** Accuracy scores are reported for ViT-B using 3 random seeds, and different datasets. CIFAR-100C refers to CIFAR-100 with the coarse setting (20 labels), while CIFAR-100F refers to the fine setting (100 labels). The "Approx." column $b_i \rightarrow b_i + n$ specify the blocks used for approximation, where the first value represents the block whose output is used to approximate the second block's output, while the "Num. Blocks" column indicates the total number of remaining blocks after the approximation. The proposed method preserves performance while reducing the number of parameters.

Approx.	Num. Params	Accuracy \uparrow				
		MNIST	F-MNIST	CIFAR-10	CIFAR-100C	CIFAR-100F
1 \rightarrow 5	60.40M	87.06 \pm 0.53	84.33 \pm 0.61	73.54 \pm 0.57	51.67 \pm 1.10	38.98 \pm 0.72
2 \rightarrow 5	66.90M	94.20 \pm 0.21	87.80 \pm 0.24	87.10 \pm 0.83	71.68 \pm 0.50	61.19 \pm 0.37
1 \rightarrow 3	73.40M	96.51 \pm 0.42	88.72 \pm 0.41	93.71 \pm 0.13	83.05 \pm 0.23	74.74 \pm 0.29
3 \rightarrow 5	73.40M	95.59 \pm 0.09	88.28 \pm 0.20	93.11 \pm 0.06	83.50 \pm 0.17	74.35 \pm 0.47
2 \rightarrow 4	73.40M	96.21 \pm 0.33	89.21 \pm 0.64	94.59 \pm 0.32	85.13 \pm 0.24	76.82 \pm 0.41
8 \rightarrow 10	73.40M	96.54 \pm 0.21	89.72 \pm 0.52	95.05 \pm 0.26	85.78 \pm 0.37	79.62 \pm 0.14
9 \rightarrow 11	73.40M	95.59 \pm 0.52	89.49 \pm 0.26	93.22 \pm 0.56	82.23 \pm 0.44	76.33 \pm 0.10
3 \rightarrow 4	79.90M	96.86 \pm 0.35	89.69 \pm 1.09	96.18 \pm 0.09	89.18 \pm 0.06	82.50 \pm 0.17
4 \rightarrow 5	79.90M	96.55 \pm 0.23	89.13 \pm 0.50	95.39 \pm 0.23	87.43 \pm 0.15	80.30 \pm 0.16
0 \rightarrow 1	79.90M	96.75 \pm 0.29	88.97 \pm 0.26	93.74 \pm 0.15	84.49 \pm 0.20	76.54 \pm 0.29
1 \rightarrow 2	79.90M	96.88 \pm 0.01	89.29 \pm 0.24	95.63 \pm 0.11	87.46 \pm 0.20	80.64 \pm 0.23
2 \rightarrow 3	79.90M	96.91 \pm 0.17	89.69 \pm 0.61	96.00 \pm 0.18	88.38 \pm 0.13	81.59 \pm 0.35
-	86.40M	<u>95.61</u> \pm 0.22	<u>89.64</u> \pm 0.57	<u>96.25</u> \pm 0.17	<u>89.52</u> \pm 0.23	<u>83.41</u> \pm 0.20

Table 8: **Image Classification Performance: RBA vs. Skip Across Seeds.** Accuracy scores for ViT-S on all the datasets are reported using 3 different seeds. The "Skip." column $b_i \rightarrow b_i + n$ specifies the blocks being skipped, where the first value represents the starting block (excluded from the skip) and the second value represents the final (included) block. The "Num. Blocks" column shows the total number of remaining blocks.

Skip	Num. Blocks	Skip Accuracy \uparrow				
		MNIST	F-MNIST	CIFAR-10	CIFAR-100C	CIFAR-100F
1 \rightarrow 5	8	92.74 \pm 0.58	82.25 \pm 0.93	58.08 \pm 0.44	43.43 \pm 0.79	32.68 \pm 0.70
2 \rightarrow 5	9	93.78 \pm 0.55	84.99 \pm 0.51	64.43 \pm 2.00	51.39 \pm 0.57	41.78 \pm 0.45
7 \rightarrow 10	9	91.56 \pm 0.46	85.02 \pm 1.15	73.94 \pm 0.34	59.99 \pm 0.73	45.00 \pm 0.31
1 \rightarrow 3	10	94.41 \pm 0.33	82.82 \pm 0.46	66.27 \pm 0.76	52.52 \pm 0.48	42.76 \pm 0.75
3 \rightarrow 5	10	93.96 \pm 0.25	86.10 \pm 0.15	74.79 \pm 1.56	62.53 \pm 0.32	54.62 \pm 0.52
2 \rightarrow 4	10	94.31 \pm 0.48	85.22 \pm 0.67	71.56 \pm 1.62	59.40 \pm 0.38	50.19 \pm 0.38
8 \rightarrow 10	10	94.82 \pm 0.21	87.77 \pm 0.43	85.74 \pm 0.32	72.39 \pm 0.41	63.79 \pm 0.66
9 \rightarrow 11	10	94.80 \pm 0.15	88.32 \pm 0.46	89.65 \pm 0.52	76.40 \pm 0.08	70.75 \pm 0.39
0 \rightarrow 1	11	95.98 \pm 0.13	84.91 \pm 0.36	70.90 \pm 0.09	57.16 \pm 0.41	47.54 \pm 0.37
1 \rightarrow 2	11	95.79 \pm 0.16	87.07 \pm 0.70	83.21 \pm 0.52	70.66 \pm 0.69	62.23 \pm 0.21
2 \rightarrow 3	11	95.14 \pm 0.39	85.50 \pm 0.62	81.24 \pm 0.48	68.63 \pm 0.33	60.22 \pm 0.75
3 \rightarrow 4	11	95.34 \pm 0.58	87.62 \pm 1.18	88.25 \pm 0.23	77.58 \pm 0.46	69.79 \pm 0.02
4 \rightarrow 5	11	95.75 \pm 0.20	87.26 \pm 0.86	86.23 \pm 0.63	74.52 \pm 0.63	66.69 \pm 0.48
5 \rightarrow 6	11	95.77 \pm 0.22	86.99 \pm 0.33	83.42 \pm 0.52	69.62 \pm 0.32	61.96 \pm 0.55
6 \rightarrow 7	11	95.33 \pm 0.08	86.64 \pm 1.14	87.57 \pm 0.24	75.91 \pm 0.20	68.70 \pm 0.31
7 \rightarrow 8	11	95.76 \pm 0.20	87.50 \pm 0.85	88.70 \pm 0.46	76.80 \pm 0.09	69.33 \pm 0.39
8 \rightarrow 9	11	96.28 \pm 0.04	88.38 \pm 0.83	89.98 \pm 0.48	76.45 \pm 0.65	71.80 \pm 0.22
9 \rightarrow 10	11	95.56 \pm 0.47	88.74 \pm 1.09	93.40 \pm 0.32	82.44 \pm 0.44	76.32 \pm 0.30
10 \rightarrow 11	11	95.22 \pm 0.29	89.39 \pm 0.30	93.77 \pm 0.69	82.39 \pm 0.06	78.68 \pm 0.29
-	12	95.95 \pm 0.40	89.01 \pm 0.63	95.87 \pm 0.08	87.60 \pm 0.15	81.29 \pm 0.20

Table 9: Generalization Results. Classification accuracy scores when approximating using a transformation calculated on other datasets for ViT-S and DiNO-S using MNIST, CIFAR-10, CIFAR-100C and CIFAR-100F. CIFAR-100C refers to CIFAR-100 with the coarse setting (20 labels), while CIFAR-100F with the fine setting (100 labels). The "Approx" column $b_i \rightarrow b_i + n$ specifies the blocks used for approximation, where the first value represents the block whose output is used to approximate the second block's output. The "Fit on" column indicates the dataset on which the linear transformation is calculated.

Encoder	Approx.	Fit On	Accuracy \uparrow			
			MNIST	CIFAR-10	CIFAR-100C	CIFAR-100F
ViT-S	2 \rightarrow 3	MNIST	94.11	57.13	41.89	28.50
		CIFAR-10	89.58	95.08	85.32	77.92
		CIFAR-100	89.63	95.00	85.50	77.74
	3 \rightarrow 4	MNIST	93.52	10.36	8.97	3.09
		CIFAR-10	88.02	95.18	86.14	78.52
		CIFAR-100	88.21	94.82	85.92	78.09
	4 \rightarrow 5	MNIST	93.96	38.40	25.56	16.52
		CIFAR-10	78.36	95.31	85.84	78.20
		CIFAR-100	80.11	94.98	86.01	78.14
	9 \rightarrow 10	MNIST	89.73	74.41	59.78	44.40
		CIFAR-10	82.28	92.39	71.63	57.17
		CIFAR-100	54.12	85.60	77.37	61.81
	1 \rightarrow 3	MNIST	92.79	16.17	11.09	3.84
		CIFAR-10	80.41	90.63	75.59	65.98
		CIFAR-100	81.24	89.98	76.27	66.26
	3 \rightarrow 5	MNIST	88.22	15.17	8.52	2.03
		CIFAR-10	61.68	93.57	80.24	71.76
		CIFAR-100	64.18	92.77	80.56	72.43
	2 \rightarrow 4	MNIST	92.74	17.24	12.27	4.27
		CIFAR-10	63.52	92.14	79.80	70.52
		CIFAR-100	66.05	91.21	79.57	70.16
	8 \rightarrow 10	MNIST	86.77	36.61	30.79	15.10
		CIFAR-10	24.29	80.81	48.73	31.74
		CIFAR-100	38.89	59.12	64.07	43.20
	9 \rightarrow 11	MNIST	77.19	31.40	18.79	4.32
		CIFAR-10	49.65	76.61	50.48	25.57
		CIFAR-100	35.61	68.40	55.67	31.59
	2 \rightarrow 5	MNIST	81.11	13.09	6.74	2.24
		CIFAR-10	37.16	88.70	67.99	57.24
		CIFAR-100	39.60	86.75	70.00	58.90
	7 \rightarrow 10	MNIST	85.04	33.28	19.26	4.59
		CIFAR-10	20.67	69.49	34.65	17.18
		CIFAR-100	30.00	48.19	53.16	26.97
	1 \rightarrow 5	MNIST	69.44	10.36	5.38	1.56
		CIFAR-10	39.49	76.98	48.11	36.38
		CIFAR-100	36.94	72.48	51.03	38.75
DiNO-S	2 \rightarrow 3	MNIST	93.04	58.24	37.95	27.62
		CIFAR-10	86.16	94.11	82.37	75.26
		CIFAR-100	86.39	93.78	82.28	75.29
	3 \rightarrow 4	MNIST	92.33	62.78	38.18	27.52
		CIFAR-10	84.70	94.37	81.93	74.69
		CIFAR-100	83.72	94.10	82.02	74.59
	4 \rightarrow 5	MNIST	91.64	57.39	36.97	26.02
		CIFAR-10	70.87	93.65	80.38	73.84
		CIFAR-100	71.51	92.98	79.96	73.54
	9 \rightarrow 10	MNIST	83.39	38.85	20.20	13.10
		CIFAR-10	45.69	88.70	61.71	50.46
		CIFAR-100	60.57	76.58	76.77	61.29
	1 \rightarrow 3	MNIST	90.60	22.30	11.76	5.47
		CIFAR-10	78.51	89.72	74.58	65.04
		CIFAR-100	79.80	89.28	74.75	64.92
	3 \rightarrow 5	MNIST	87.54	24.55	11.93	6.67
		CIFAR-10	63.66	87.17	66.16	58.36
		CIFAR-100	64.26	84.40	66.43	58.51
	2 \rightarrow 4	MNIST	90.54	19.14	9.99	4.99
		CIFAR-10	62.32	88.03	68.53	59.23
		CIFAR-100	64.89	86.98	68.54	59.15
	8 \rightarrow 10	MNIST	80.88	22.27	10.30	6.25
		CIFAR-10	25.67	85.07	48.44	35.42
		CIFAR-100	29.81	67.51	67.59	47.97
	9 \rightarrow 11	MNIST	27.79	9.93	7.30	1.67
		CIFAR-10	15.94	59.66	19.22	7.62
		CIFAR-100	15.71	40.73	32.06	12.17
	2 \rightarrow 5	MNIST	82.67	10.77	5.85	2.85
		CIFAR-10	49.78	73.83	46.89	38.80
		CIFAR-100	48.24	67.62	46.85	38.36
	7 \rightarrow 10	MNIST	75.50	15.89	10.43	4.24
		CIFAR-10	17.75	76.55	36.68	21.94
		CIFAR-100	19.13	53.86	55.80	33.79
	1 \rightarrow 5	MNIST	68.07	11.29	6.29	1.74
		CIFAR-10	49.25	56.93	31.06	22.86
		CIFAR-100	47.81	47.83	30.78	21.78